

Spontaneous (Anti)meron Chains in the Domain Walls of van der Waals Ferromagnetic $\text{Fe}_{5-x}\text{GeTe}_2$

Yang Gao, Qiangwei Yin, Qi Wang, Zhuolin Li, Jianwang Cai, Tongyun Zhao, Hechang Lei,* Shouguo Wang,* Ying Zhang,* and Baogen Shen

The promise of topologically vortex-like magnetic spin textures hinges on the intriguing physical properties and theories in fundamental research and their distinguished roles as high-efficiency information units in future spintronics. The exploration of such magnetic states with unique spin configurations has never ceased. In this study, the emergence of unconventional (anti)meron chains from a domain wall pair is directly observed at zero field in 2D ferromagnetic $\text{Fe}_{5-x}\text{GeTe}_2$, closely correlated with significant enhancement of the in-plane magnetization and weak van der Waals interactions. The simultaneous appearance of a large topological Hall effect is observed at the same temperature range as that of the abnormal magnetic transition. Moreover, the distinctive features of the (anti)meron chains and their collective dynamic behavior under external fields may provide concrete experimental evidence for the recent theoretical prediction of the magnetic-domain-wall topology and endorse a broader range of possibilities for electronics, spintronics, condensed matter physics, etc.

Resurgent research on the magnetic vortex^[1–3] and vortex-like spin configurations including the (anti)skyrmion,^[4–6] biskymion,^[7,8] (anti)meron,^[9–11] and bobber^[12] has resulted in significant progress in fundamental research and the exploration

Y. Gao, Z. L. Li, Prof. J. W. Cai, Prof. T. Y. Zhao, Prof. Y. Zhang, Prof. B. G. Shen
Beijing National Laboratory for Condensed Matter Physics and Institute of Physics

Chinese Academy of Sciences
Beijing 100190, China
E-mail: zhangy@iphy.ac.cn

Y. Gao, Prof. S. G. Wang
Institute of Advanced Materials
Beijing Normal University
Beijing 100875, China
E-mail: sgwang@bnu.edu.cn

Q. W. Yin, Q. Wang, Prof. H. C. Lei
Department of Physics and Beijing Key Laboratory of Opto-Electronic Functional Materials & Micro-Nano Devices
Renmin University of China
Beijing 100872, China
E-mail: hlei@ruc.edu.cn

Z. L. Li, Prof. B. G. Shen
School of Physical Sciences
University of Chinese Academy of Sciences
Beijing 100049, China
Prof. Y. Zhang
Songshan Lake Materials Laboratory
Dongguan, Guangdong 523808, China

 The ORCID identification number(s) for the author(s) of this article can be found under <https://doi.org/10.1002/adma.202005228>.

DOI: 10.1002/adma.202005228

of spintronics. Each topological texture exhibits a unique topological number N in the form of a lattice or isolated quasiparticle, offering the capability of encoding information bits with dense integration and low energy cost in nanodevices.^[13,14] It was found that the generation and application of such topological spin textures build strong correlations with spin-orbit coupling, competition among magnetic interactions, and emergent electromagnetic properties,^[13–16] which assist the understanding of the underlying mechanism and the exploration of new spin states and materials. Thereafter, the host material and generation mechanisms have been extended from the initial chiral magnets with Dzyaloshinskii–Moriya interaction (DMI)^[4–6] to centrosymmetric magnets with uniaxial magnetic anisotropy^[7,8] and

to magnetic multilayers with interfacial DMI.^[17,18] Unless external manipulation or the proliferation of defects promote their existence at zero field,^[19–22] vortex-like spin textures can only be obtained as an excitation state under the stimuli of certain magnetic fields. The corresponding magnetic ground state exhibits a periodic helical spin order with uniform stripe domains. Although the generation mechanisms appear different, the fundamental origin of such nonlinear magnetization textures can be ascribed to the canting state of the spin moments introduced by appropriate energy competition among the different magnetic interactions. Considering the spin orientation, the magnetic moment variation within the conventional 180° or 90° domain wall resembles half or quarter of the sinusoidal spin period of a helical stripe domain^[23] and shares the same classification criteria (Bloch or Néel type). However, topological spin textures from conventional domain walls have not yet been experimentally observed, although recent theoretical studies have predicted domain wall skyrmions.^[24,25]

The discovery of out-of-plane anisotropy and strong electron correlation effects by lifting the Mermin–Wagner restriction in the van der Waals (vdW) itinerant ferromagnet (FM) Fe–Ge–Te ^[26–31] is a new starting point for exploring interesting spin structures. It has been demonstrated that the structure of cleavable Fe–Ge–Te building blocks and variable interlayer vdW interactions are tunable parameters for controlling the magnetic properties.^[26,29] The different atomic arrangements of Fe and Ge atoms with unique Fe vacancies in the Fe–Ge–Te slabs of $\text{Fe}_{5-x}\text{GeTe}_2$ result in more complicated physical properties and higher Curie temperature ($260\text{–}310\text{ K}$)^[29–31] than the

well-studied $\text{Fe}_{3-x}\text{GeTe}_2$ (150–240 K),^[26–28] prompting the exploration of the mysterious magnetization origination and the fascinating functionality of $\text{Fe}_{5-x}\text{GeTe}_2$.

In this study, we experimentally demonstrate the evolution of (anti)merons in the distinctive form of a line chain from the 180° domain wall pair in $\text{Fe}_{5-x}\text{GeTe}_2$. A periodic array of magnetic (anti)merons with high linear density is spontaneously generated within a certain temperature range, without requiring an external magnetic field or DMI. Based on detailed measurements of the magnetization and magnetotransport properties, we propose a tentative explanation of its origin. Furthermore, we reveal the stability and dynamic behavior of the obtained (anti)meron chains under external stimuli including electrical voltage and magnetic fields.

Figure 1a presents the structure of centrosymmetric ferromagnet $\text{Fe}_{5-x}\text{GeTe}_2$ with a rhombohedral $R\bar{3}m$ space group,^[29] where the Fe–Ge–Te layers stack along the c -axis with weak interlayer vdW interaction. In $\text{Fe}_{5-x}\text{GeTe}_2$, the Fe(2) and Fe(3) positions are fully occupied, but the Fe(1) site has significant iron vacancies.^[29,31] The Ge position splits into two sites to maintain an appropriate bond distance between Fe(1) and Ge.^[29–31] The absence of impurities was confirmed from the X-ray diffraction (XRD) pattern, and the Fe vacancies were identified as $\text{Fe}_{4.78(4)}\text{GeTe}_{2.13(1)}$, when setting the content of Ge as 1 based on the energy-dispersive X-ray (EDX) spectrum (Figure S1, Supporting Information). In Figure 1, the magnetic transition can be directly observed, and is characterized in a thin plate of single-crystal $\text{Fe}_{5-x}\text{GeTe}_2$ along the $(1\bar{1}0)$ zone-axis through in situ cooling, with Lorentz transmission

electron microscopy (L-TEM). The dot domains gradually evolve from the conventional 180° domain wall pair and are well separated at 180 K (Figure 1d), exhibiting small size (≈ 20 nm) and high linear density (≈ 24 per μm) along each domain wall.

The enlarged lateral magnetic component distributions (Figure 1b,e) are realized from the dot domains in the selected boxes using transport-of-intensity equation (TIE) analysis (details are provided in the Experimental Section). Chains of topological spin configurations with uniform counterclockwise (CCW) and clockwise (CW) helicities are observed alternating in each domain wall pair. The colors and arrows denote the directions of the in-plane magnetization according to the color wheel with a dark color indicating out-of-plane magnetization in the core. Although the definite out-of-plane direction cannot be determined through L-TEM, the polarity should have the same inward (meron) or outward (antimeron) magnetization direction for each domain wall according to the (anti)meron definition^[32] and chirality conservation in centrosymmetric $\text{Fe}_{5-x}\text{GeTe}_2$. Here, we demonstrate the meron pair schematics with inward magnetic moments in the core region alone, and use an (anti)meron pair to present the equal possibility of a meron or antimeron pair. The spin configuration with inward (meron) or outward (antimeron) magnetic moments in the core region and in-plane moments near the peripheries is the dissociation of a skyrmion; therefore, it exhibits a fractional topological number.^[9,11,33] Spin configurations with naturally half-period helical magnetization across the Bloch-type 180° domain wall were extracted from the 3D structures (Figure 1f)

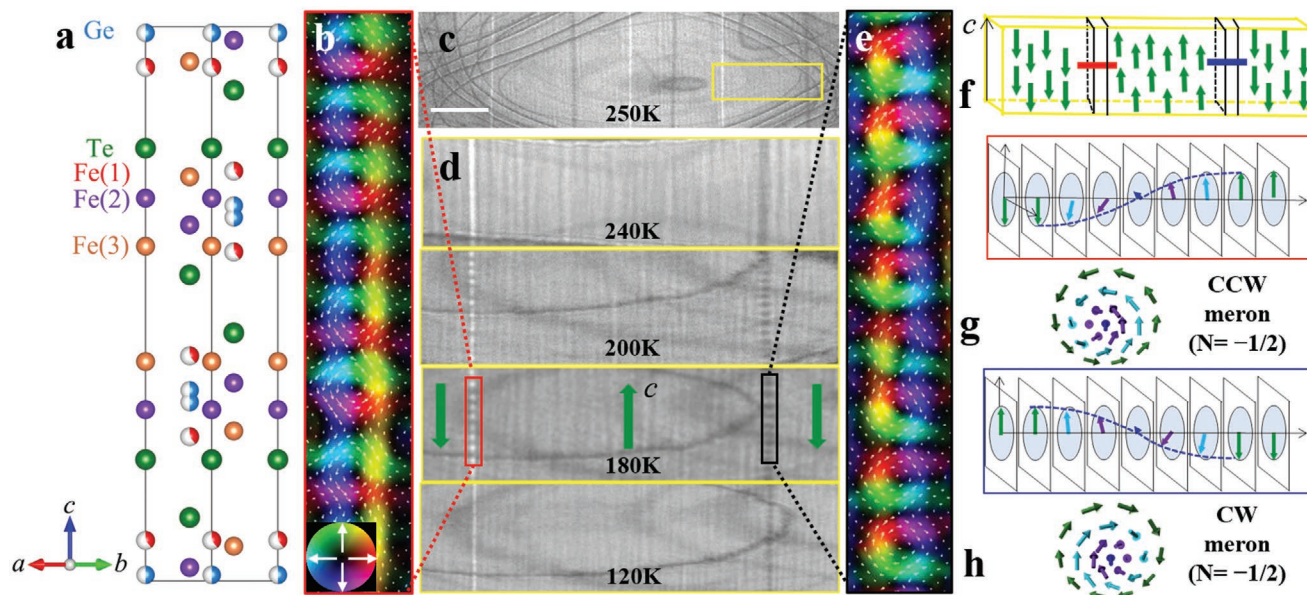


Figure 1. (Anti)meron chains in the domain wall pair of van der Waals $\text{Fe}_{5-x}\text{GeTe}_2$. a) Crystal structure of $\text{Fe}_{5-x}\text{GeTe}_2$ with the Fe–Ge–Te layers stacked along the c -axis; the Fe(1) and Ge positions are partially occupied (marked by the color difference). b, e) Magnified magnetization texture of the selected region in the domain wall pair at 180 K based on the transport-of-intensity equation (see Experimental Section; the arrows and color scale indicate the direction and magnitude of the in-plane magnetization, respectively). c) Under-focused L-TEM image with three pairs of 180° domain walls along the c -axis at 250 K (scale bar = $1 \mu\text{m}$). d) Real-space observation of (anti)meron evolution from a conventional domain wall pair (focusing on the yellow box region in c) with the decrease in temperature (the green arrow indicates the dominant magnetization direction within the domains). f) Schematic of the 3D magnetic domains with 180° domain wall pair. g, h) Cross-sectional schematics of the swirling magnetization across the Bloch-type domain wall and the corresponding evolved topological textures with counterclockwise (CCW) and clockwise (CW) helicities, highlighting their spin correlation. The schematic spin configuration with inward magnetic moments in the core region is demonstrated as a meron pair with a topological number $N = -1/2$.

and are schematically depicted in Figure 1g,h. Analogous to the evolution from the sinusoidal period of helical spin modulation to skyrmions, the corresponding counterclockwise (CCW) and clockwise (CW) meron pair with a topological number $N = -1/2$ is demonstrated, highlighting the spin correlation with domain wall constriction.

The L-TEM images in Figure 1c,d show the sequential transformation from the conventional 180° domain wall to an (anti)meron chain, below the Curie temperature T_c (≈ 275 K; focusing on the single-domain wall pair in Figure 1d). It should be noted that the experiments were conducted without any external magnetic fields, and the transformation was reversible. The conventional 180° domain wall pair with white and dark contrast begins to break into a series of magnetic (anti)meron pairs below ≈ 250 K, while the dominant domain magnetization (green arrow along the c -axis) appears unchanged. The magnetic (anti)merons are well separated, particularly in the temperature range of 230–130 K, subsequently merging into the continuous domain wall at lower temperatures. The 180° domains with dominant magnetization along the c -axis correspond to the maze domain structure near the [001] zone-axis due to c -axial magnetic anisotropy, which is similar to that of $\text{Fe}_{3-x}\text{GeTe}_2$ (Figure S2, Supporting Information). However, the (anti)meron transformation is unique in $\text{Fe}_{5-x}\text{GeTe}_2$ and is not observed in $\text{Fe}_{3-x}\text{GeTe}_2$, where the conventional 180° domain

wall remains invariant, when the temperature decreases (Figures S3 and S4, Supporting Information).

To determine the generation mechanism of the (anti)meron chains in $\text{Fe}_{5-x}\text{GeTe}_2$, the temperature dependence of magnetic susceptibilities $\chi_{ab}(T)$ for $H//ab$ and $\chi_c(T)$ for $H//c$ are measured, as shown in Figure 2. With the decrease in temperature, $\chi_c(T)$ at $\mu_0 H = 0.01$ T exhibits weak temperature dependence after a rapid increase near T_c (Figure 2a), consistent with the invariant domain structure on the plane near the [001] zone-axis. In contrast, $\chi_{ab}(T)$ in the same field exhibits significant enhancement of the in-plane magnetization in a certain temperature range. A small spike emerges at approximately $T = 258$ K, coupled with the onset of (anti)meron chains generated from the domain wall pair. The broad cusp with a maximum value at ≈ 180 K agrees well with the distribution of the well-separated (anti)meron pairs in Figure 1d. Finally, with the further decrease in temperature to $T < 100$ K, $\chi_{ab}(T)$ abruptly reduces and becomes comparable with $\chi_c(T)$. Correspondingly, the domain-wall-(anti)meron-chain state disappears. In addition, the isothermal $M(\mu_0 H)$ curves at different temperatures for both field directions (Figure 2b) reflect the evolution of magnetic anisotropy. At high temperatures, the difference in the saturation field $\mu_0 H_s$ between $M_{ab}(\mu_0 H)$ and $M_c(\mu_0 H)$ is small. However, from 100 to 260 K, the smaller $\mu_0 H_s$ for $H//ab$ compared to $H//c$ implies that the magnetic moments align

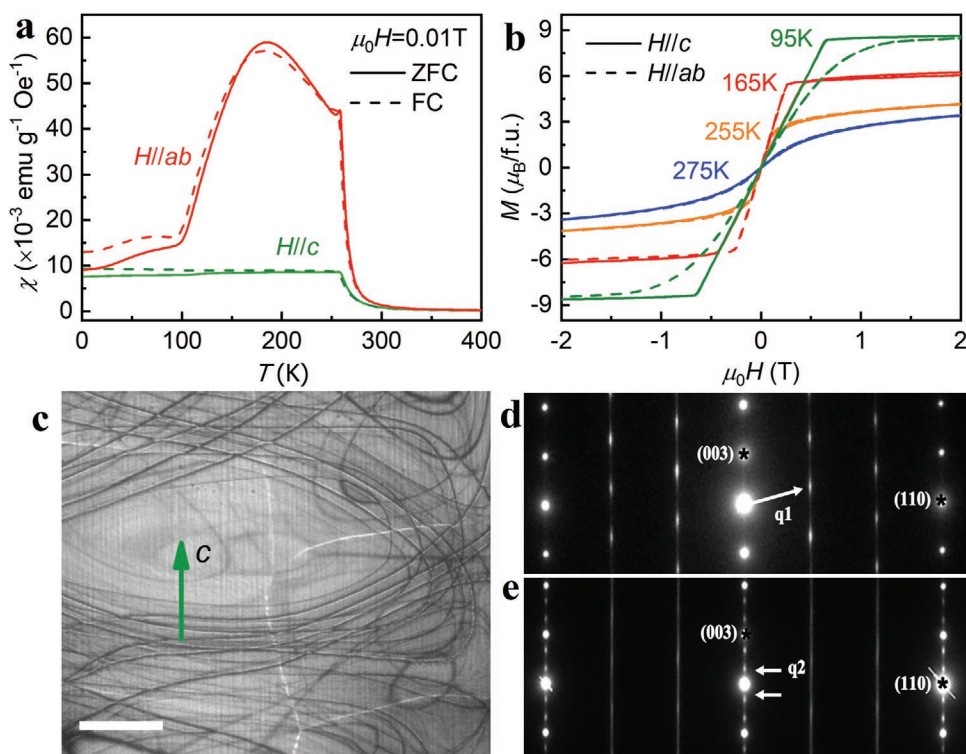


Figure 2. Origin of the domain-wall (anti)meron chains in $\text{Fe}_{5-x}\text{GeTe}_2$. a) Temperature dependence of the magnetic susceptibility $\chi(T)$ upon cooling with a magnetic field of 0.01 T applied along $H//c$ and $H//ab$, respectively. The significant enhancement of $\chi_{ab}(T)$ versus the weak temperature dependence of $\chi_c(T)$ is detected, in good agreement with the temperature range of the (anti)meron chain. b) Field dependence of magnetization $M(\mu_0 H)$ for $H//c$ and $H//ab$ at various temperatures, with the magnetization switching to the dominant in-plane component at a representative temperature of 165 K. c) Magnetic domains with the coexistence of magnetizations parallel and perpendicular to the c -axis at certain regions (scale bar = 1 μm). d,e) Selected-area electron diffraction patterns along the $[1\bar{1}0]$ zone-axis with superstructure modulation vector $q_1 = \pm 1/3(1, 1, 3)$ and $q_2 = \pm 3/10(0, 0, 3l)$ at a temperature above and below 100 K, respectively. The structural difference in correlation with the Fe(1) ordering contributes to the enhancement and diminishment of the in-plane magnetization component, when the temperature is changed.

more easily along the ab plane, which could result in additional rearrangement of the magnetic domains, if the in-plane magnetization component is sufficiently high (Figure 2c). The $\mu_0 H_s$ trend for these two field directions is reversed below 100 K, that is, the easy axis of magnetization becomes the c -axis. Therefore, with the significant enhancement of the in-plane magnetization to introduce magnetic competition, the generation of (anti)merons is anticipated because several experimental and theoretical studies have emphasized that magnetic anisotropy alternation could energetically promote the topological (anti)meron state.^[9,11] In comparison with the homogeneous lattice configuration under external magnetic fields in the DMI-requirement chiral magnets, a distinguished form of the (anti)meron chain is spontaneously generated in the local domain wall by simply decreasing the temperature in centrosymmetric $\text{Fe}_{5-x}\text{GeTe}_2$.

The changes in the in-plane magnetic properties could be closely related to the local magnetic/structural ordering of the Fe(1) position in $\text{Fe}_{5-x}\text{GeTe}_2$.^[26] Electron diffraction with modulation $q_1 = \pm 1/3(1, 1, 3)$ and the diffused line along $1/3(1, 1, l)$ at the $[1\bar{1}0]$ zone-axis (Figure 2d) directly reflect the dominant in-plane or canted supercell structure without significant ordering along the c -axis above 100 K. Such electron diffraction modulation is primarily introduced by the intraplane ordering of the vacancies at the Fe(1) site,^[29] which could lead to significant enhancement of the in-plane magnetization component. The Mössbauer spectra also reveal that the Fe(1) moments fluctuate too rapidly along the c -axis to form ordering above 100 K according to the dynamic model.^[29] However, below 100 K, additional q_2 modulation spots with a wavevector $q_2 = \pm 3/10(0, 0, 3l)$ (12 K in Figure 2e) indicate the emergence of a specific long-range superstructure along the c -axis, accompanied by a first-order transition.^[29] After the c -axial Fe(1) moments become statically ordered because of the interplane vacancy ordering of the Fe(1) site at temperatures below 100 K, they could considerably suppress the in-plane magnetization component and present an abrupt reduction in $\chi_{ab}(T)$, resulting in the disappearance of the (anti)meron chains. These simultaneous phenomena indicate that weak ordering correlation together with weak vdW interaction along the c -axis are crucial for the isolation of the topological domains; otherwise, continuous domain walls with cross-tie-wall features would remain.^[33] Therefore, the energy competition during magnetization changes from the c -axis to the ab plane; the weak interaction along the c -axis and the distinctive spin features of the domain wall jointly result in the generation of isolated (anti)meron pairs.

Magnetotransport measurements also partially reflect the evolution of the topological spin textures and magnetic/structural orderings in $\text{Fe}_{5-x}\text{GeTe}_2$ (Figure 3). When $T < T_c$, besides the ordinary Hall resistivity ρ_{yx}^N and the intrinsic anomalous Hall resistivity ρ_{yx}^A , the topological Hall resistivity ρ_{yx}^T also contributes to the total Hall resistivity $\rho_{yx}(\mu_0 H)$ ^[15,34,35] (Figure S5, Supporting Information). As shown in Figure 3a,b, when T is close to T_c , the derived ρ_{yx}^T is small and its intensity increases with the decrease in temperature, reaching a maximum value $\rho_{yx}^{T,\text{max}}$ of $\approx -0.74 \mu\Omega \text{ cm}$ at $\approx 220 \text{ K}$ and 0.2 T . With the further decrease in temperature, ρ_{yx}^T rapidly decreases with the shift in the peak position to higher fields. Below 100 K, significantly different shapes and small values are observed in the field

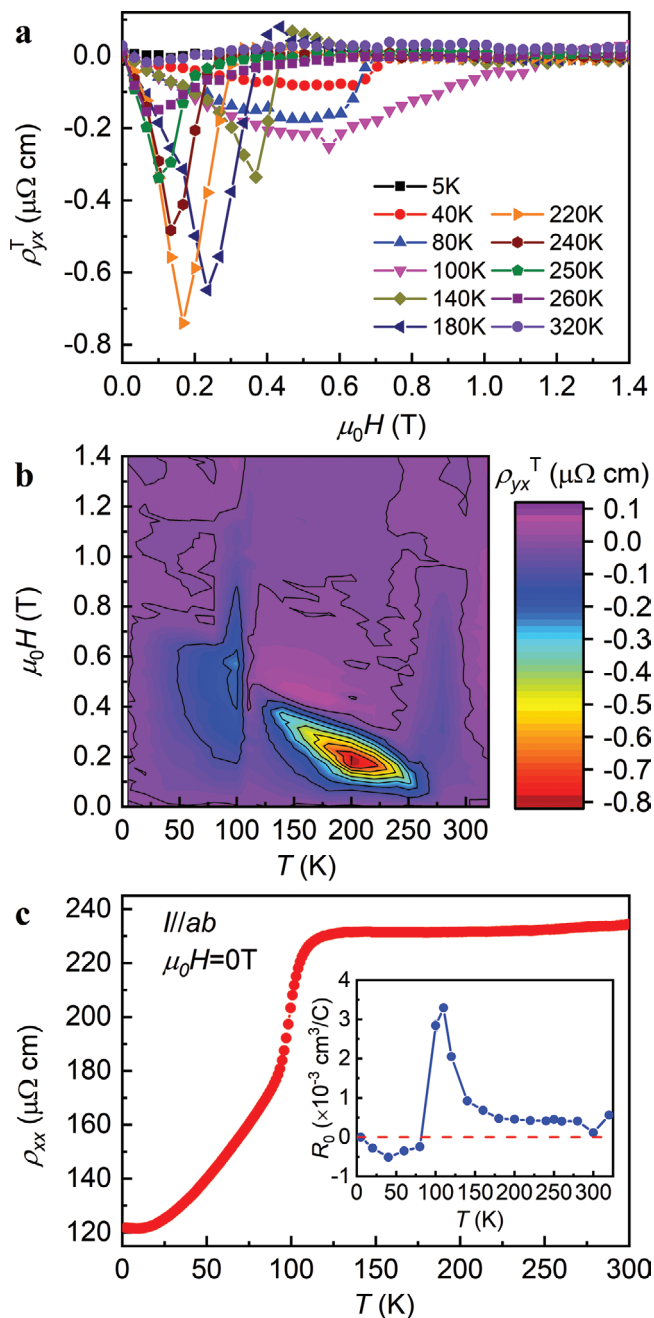


Figure 3. Simultaneous magnetotransport response in $\text{Fe}_{5-x}\text{GeTe}_2$. a) Field dependence of the topological Hall resistivity $\rho_{yx}^T(T)$ at different temperatures in good correlation with the microscopic domain evolution temperature range in ferromagnetic $\text{Fe}_{5-x}\text{GeTe}_2$. b) Contour plot of $\rho_{yx}^T(T, \mu_0 H)$ for T ranging from 5 to 320 K and $\mu_0 H$ ranging from 0 to 1.4 T. c) Zero-field longitudinal resistivity $\rho_{xx}(T)$ as a function of the temperature. Inset: temperature dependence of the fitted normal Hall coefficient $R_0(T)$. The sign changes from positive at high temperatures ($T > 110 \text{ K}$) to negative at low temperatures, suggesting a dominant carrier type shift from holes to electrons with the lowering of the temperature.

dependence of ρ_{yx}^T . The negative values (dips) of the $\rho_{yx}^T(\mu_0 H)$ curve in Figure 3a suggest that the sign of the spin polarization (P) of the charge carriers or the emergent field induced by the topologically nontrivial spin texture ($\mu_0 H_z$) is negative because

ρ_{yx}^T is proportional to P and $\mu_0 H_z$, which has been frequently observed in various materials with topological spin excitations and nonlinear magnetization.^[8,36] Moreover, $\mu_0 H_z$ is highest, when the nonlinear spin excitations are maximum at a certain optimal magnetic field; further increase in the field suppresses the topological spin texture through complete spin polarization, resulting in a dip in the field dependence of the $\rho_{yx}^T(\mu_0 H)$ curve. Therefore, the simultaneous emergence of large ρ_{yx}^T and domain-wall (anti)meron chains evidences the close relationship between them and manifests a nontrivial topological electromagnetic response in $\text{Fe}_{5-x}\text{GeTe}_2$.

On the other hand, the zero-field longitudinal resistivity $\rho_{xx}(T)$ changes drastically near 100 K. It exhibits weak temperature dependence when $T > 125$ K (Figure 3c) but drops significantly at lower temperatures. The normal Hall coefficient R_0 derived from the field dependence of $\rho_{yx}^N(\mu_0 H)$ (Figure S5, Supporting Information) is positive at high temperatures ($T > 100$ K) and becomes negative at low temperatures, strongly suggesting that the dominant carrier type changes from holes to electrons with the decrease in temperature. In addition, the anomalous Hall coefficient R_s rapidly decreases below ≈ 110 K, whereas the negative magnetoresistance (MR) reaches a maximum value at 110 K (approximately -16% at 5 T; Figure S5, Supporting Information). All these results strongly suggest that the ordering of the Fe(1) sublattice not only changes the magnetic anisotropy to induce the domain-wall-(anti)meron-chain state, but also contributes to drastic changes in the electron-spin scattering rate, electron structure, and Fermi surface.^[29,30] Thus, there is strong coupling between the generation of (anti)meron chains and the changes in the crystal structure, magnetism, and electronic structure in $\text{Fe}_{5-x}\text{GeTe}_2$.

Next, we investigate the stability and dynamic behavior of the domain-wall (anti)meron chain under stimuli such as electrical voltage and magnetic fields (schematics in Figure 4a,d, respectively) near the $[1\bar{1}0]$ zone-axis. The L-TEM images in Figure 4b are extracted from the in situ video, when voltages are applied at different temperatures (Video S1, Supporting Information). The collective domain wall shift is dominant, if the complete (anti)meron state is obtained; otherwise, additional (anti)meron nucleation along with collective mobility is discerned. The meron pair chains move along the same direction with a change in the interval distance from the initial $1.4 \mu\text{m}$ (Figure 4b) to $1.1 \mu\text{m}$ (Figure 4c) after the application of 5 V at 200 K, which may be caused by the topological Magnus force on the meron pair due to the same topological number.^[18] Collective movement of the domain-wall (anti)meron chain appears easier to initiate through the c -axial magnetic field than through electrical stimuli (Figure S6, Supporting Information). A magnetic field along the c -axis is introduced by slightly tilting the sample relative to the perpendicular magnetic field of 0.02 T. Figure 4e,f show significant position change in the magnetic (anti)meron chain at tilting angles of 4° and -12° , respectively. The overall distance dependence of the tilting angle is summarized in Figure 4g. The domain-wall (anti)meron chain can be modulated back and forth before reaching a minimum distance of ≈ 200 nm, where the meron pair collides with each other and is annihilated. This critical exchange length envisages further domain-wall (anti)meron manipulation and simulation. The collective behavior for the topological Hall effect is intriguing

and further manifests the relativistic theories on the dynamics of domain-wall textures such that configurations remain intact in the wall during motion under external perturbation.^[24,25]

In summary, we directly demonstrated the emergence of a novel (anti)meron chain from the conventional 180° domain wall pair by decreasing the temperature at zero field in $\text{Fe}_{5-x}\text{GeTe}_2$. The exotic features of the (anti)meron chain without DMI and its collectively dynamic behavior experimentally demonstrate a novel mechanism for topological texture generation in the domain wall. The discovery of a tunable domain-wall topology in vdW centrosymmetric $\text{Fe}_{5-x}\text{GeTe}_2$ can shed light on the fascinating mechanism and its functionality as a new paradigm for electronics, spintronics storage, etc.

Experimental Section.

Sample Synthesis, Structure, and Composition Characterization: Single crystals of $\text{Fe}_{5-x}\text{GeTe}_2$ were grown through the chemical vapor transport method with iodine as the transport agent. High-purity Fe (powder), Ge (powder), and Te (grain) were taken in a stoichiometric molar ratio of 5:1:2 and placed in an evacuated quartz tube together with 50 mg of iodine. The tube was heated to 1050°C for 10 h and the temperature was maintained for 6 h; it was then cooled to 760°C at a rate of 5°C h^{-1} , and the temperature was maintained for 50 h and then quenched. Shiny crystals with typical sizes of approximately $3 \times 2 \times 0.05 \text{ mm}^3$ (length \times width \times thickness) were obtained. Single crystal XRD patterns were acquired using a Bruker D8 X-ray diffractometer with Cu K_α radiation ($\lambda = 0.15418 \text{ nm}$) at room temperature of 298 K. The elemental analysis was performed using EDX spectroscopy analysis in a FEI Nano 450 scanning electron microscope.

Transport and Magnetization Characterization: The magnetization and electrical transport measurements were performed using a Quantum Design MPMS3 and PPMS-14T, respectively. The longitudinal and Hall electrical resistivity were measured simultaneously using a standard five-probe configuration in a bulk single crystal sized of $1.9 \times 0.9 \times 0.05 \text{ mm}^3$ (length \times width \times thickness). In order to effectively eliminate the influence of voltage probe misalignment, the resistivity was measured in both positive and negative fields. The final longitudinal and Hall resistivity values were obtained by symmetrizing and antisymmetrizing the raw data.

Lorentz TEM Measurements: The magnetic domain wall contrast was observed by using a JEOL-dedicated Lorentz TEM (JEOL2100F). Liquid-nitrogen and liquid-helium holder was used for temperature manipulation. The voltage-driven behavior of (anti)meron chain was conducted by probe touching the sample in a voltage-combined liquid-nitrogen TEM holder. The external perpendicular magnetic field was introduced by gradually increasing the objective lens current. The magnetic domain wall contrast at different focus was imaged under the convergent or divergent electron beam, which was introduced by the interaction of electron beam with the in-plane magnetization. To determine the in-plane magnetization distribution of a topological texture, the three sets of images with under-, over-, and just (or zero) focal lengths were recorded by a charge coupled device (CCD) camera and then the high-resolution in-plane magnetization distribution map was obtained using commercial software QPt, which enabled to work out phase images and then created magnetic field images on the basis of the TIE equation. The colors and arrows depicted the magnitude and orientation of the in-plane magnetization according to the color wheel. The crystalline orientation for the grain was checked by selected-area electron diffraction. The specimen along $[1\bar{1}0]$ and $[001]$ zone-axis for L-TEM observation was respectively prepared via focused ion beam milling and traditional polishing, dimpling, and subsequently, ion milling. The thickness of L-TEM specimen was about 50 nm, which was measured by electron energy loss spectrum.

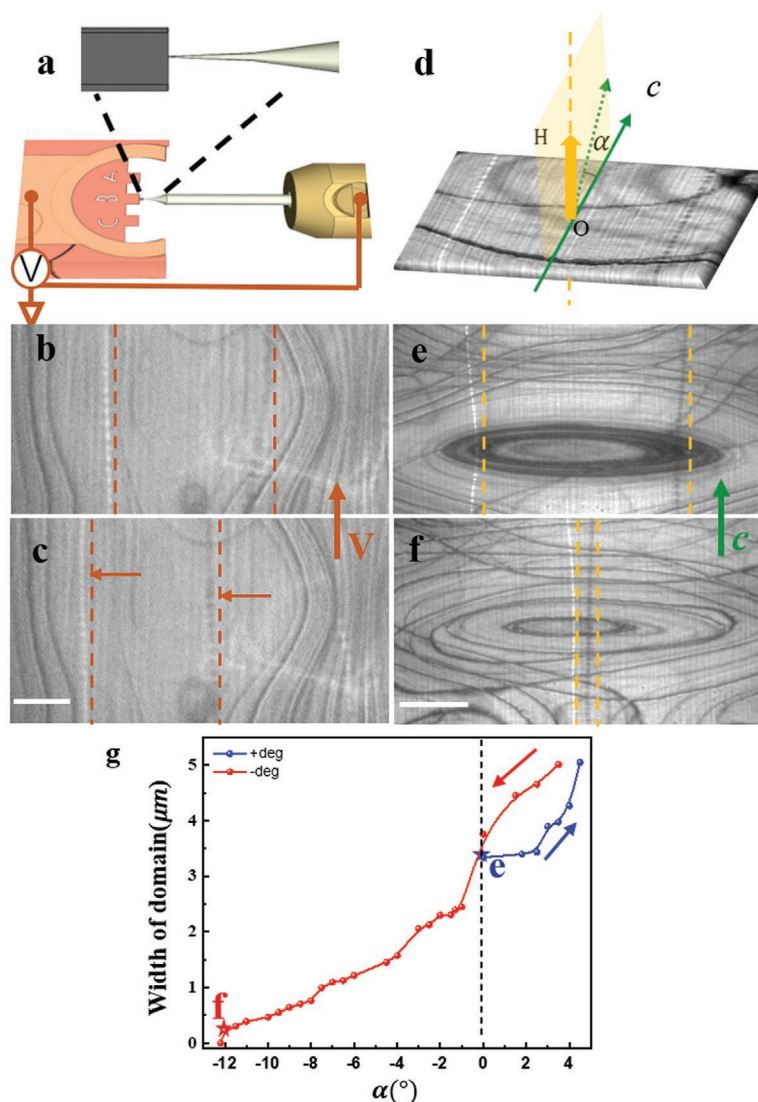


Figure 4. Dynamic behavior of (anti)meron chains. a) Schematic illustration of the application of electrical voltage to the sample. b,c) Position change of the (anti)meron chain before and after collective movement in the same direction under the application of voltage, respectively. d) Schematic illustration of the introduction of a magnetic field along the c -axis by tilting the sample. e,f) Distribution of the (anti)meron chains after collective domain wall shift at angles of 4° and -12° relative to a perpendicular magnetic field of 0.02 T, respectively (scale bar: 500 nm). g) Overall distance dependence of the domain wall (anti)merons on the tilting angle due to collective movement.

Supporting Information

Supporting Information is available from the Wiley Online Library or from the author.

Academy of Sciences (Grant No. FJCY18040302), and Youth Innovation Promotion Association (CAS 2015004). All data needed to evaluate the conclusions in the paper are present in the paper and the supplementary materials.

Acknowledgements

The authors thank Y. Zhou, Z. Y. Meng, S. Meng, J. Lu, and L. Yu for theoretical discussions. This work was supported by the National Key R&D Program of China (Grants Nos. 2018YFE0202600, 2016YFA0300504), the National Natural Science Foundation of China (Nos. 11874408, 11774423, 11822412, and 51625101), the Fundamental Research Funds for the Central Universities and the Research Funds of Renmin University of China (RUC) (18XNLG14 and 19XNLG17), the Strategic Priority Research Program of Chinese Academy of Sciences (Grant No. XDB33030100), Fujian Institute of Innovation, Chinese

Conflict of Interest

The authors declare no conflict of interest.

Author Contributions

Y.G. and Q.W.Y. contributed equally to this work. H.C.L. and Y.Z. supervised the project. Q.W.Y., Q.W., and H.C.L. synthesized the single crystals and carried out structural characterization, transport, and

magnetization measurements; Y.G., Z.L.L., and Y.Z. performed magnetic domain and dynamic behavior experiments via Lorentz TEM. Y.G., Q.W.Y., H.C.L., and Y.Z. analyzed the experimental data and plotted the figures; H.C.L. and Y.Z. wrote the manuscript after discussing data with J.W.C., T.Y.Z., B.G.S., and S.G.W. and with all the authors.

Keywords

domain-wall topology, $\text{Fe}_{5-x}\text{GeTe}_2$, meron chains, van der Waals ferromagnets

Received: August 1, 2020

Revised: October 3, 2020

Published online:

-
- [1] F. Wilczek, *Nat. Phys.* **2009**, *5*, 614.
- [2] R. M. Lutchyn, E. P. A. M. Bakkers, L. P. Kouwenhoven, P. Krogstrup, C. M. Marcus, Y. Oreg, *Nat. Rev. Mater.* **2018**, *3*, 52.
- [3] S. Zhu, L. Kong, L. Cao, H. Chen, M. Papaj, S. Du, Y. Xing, W. Liu, D. Wang, C. Shen, F. Yang, J. Schneeloch, R. Zhong, G. Gu, L. Fu, Y.-Y. Zhang, H. Ding, H.-J. Gao, *Science* **2020**, *367*, 189.
- [4] X. Z. Yu, Y. Onose, N. Kanazawa, J. H. Park, J. H. Han, Y. Matsui, N. Nagaosa, Y. Tokura, *Nature* **2010**, *465*, 901.
- [5] S. Muhlbauer, B. Binz, F. Jonietz, C. Pfleiderer, A. Rosch, A. Neubauer, R. Georgii, P. Boni, *Science* **2009**, *323*, 915.
- [6] A. K. Nayak, V. Kumar, T. Ma, P. Werner, E. Pippel, R. Sahoo, F. Damay, U. K. Rößler, C. Felser, S. S. P. Parkin, *Nature* **2017**, *548*, 561.
- [7] X. Z. Yu, Y. Tokunaga, Y. Kaneko, W. Z. Zhang, K. Kimoto, Y. Matsui, Y. Taguchi, Y. Tokura, *Nat. Commun.* **2014**, *5*, 3198.
- [8] W. Wang, Y. Zhang, G. Xu, L. Peng, B. Ding, Y. Wang, Z. Hou, X. Zhang, X. Li, E. Liu, S. Wang, J. Cai, F. Wang, J. Li, F. Hu, G. Wu, B. Shen, X.-X. Zhang, *Adv. Mater.* **2016**, *28*, 6887.
- [9] X. Z. Yu, W. Koshibae, Y. Tokunaga, K. Shibata, Y. Taguchi, N. Nagaosa, Y. Tokura, *Nature* **2018**, *564*, 95.
- [10] S. Wintz, C. Bunce, A. Neudert, M. Körner, T. Strache, M. Buhl, A. Erbe, S. Gemming, J. Raabe, C. Quitmann, J. Fassbender, *Phys. Rev. Lett.* **2013**, *110*, 177201.
- [11] S.-Z. Lin, A. Saxena, C. D. Batista, *Phys. Rev. B* **2015**, *91*, 224407.
- [12] F. Zheng, F. N. Rybakov, A. B. Borisov, D. Song, S. Wang, Z.-A. Li, H. Du, N. S. Kiselev, J. Caron, A. Kovács, M. Tian, Y. Zhang, S. Blügel, R. E. Dunin-Borkowski, *Nat. Nanotechnol.* **2018**, *13*, 451.
- [13] N. Nagaosa, Y. Tokura, *Nat. Nanotechnol.* **2013**, *8*, 899.
- [14] A. Fert, V. Cros, J. Sampaio, *Nat. Nanotechnol.* **2013**, *8*, 152.
- [15] T. Schulz, R. Ritz, A. Bauer, M. Halder, M. Wagner, C. Franz, C. Pfleiderer, K. Everschor, M. Garst, A. Rosch, *Nat. Phys.* **2011**, *7*, 713.
- [16] A. Neubauer, C. Pfleiderer, B. Binz, A. Rosch, R. Ritz, P. G. Niklowitz, P. Böni, *Phys. Rev. Lett.* **2009**, *102*, 186602.
- [17] G. Chen, T. Ma, A. T. N'diaye, H. Kwon, C. Won, Y. Wu, A. K. Schmid, *Nat. Commun.* **2013**, *4*, 2671.
- [18] W. Jiang, G. Chen, K. Liu, J. Zang, S. G. E. te Velthuis, A. Hoffmann, *Phys. Rep.* **2017**, *704*, 1.
- [19] U. K. Rößler, A. N. Bogdanov, C. Pfleiderer, *Nature* **2006**, *442*, 797.
- [20] K. Karube, J. S. White, N. Reynolds, J. L. Gavilano, H. Oike, A. Kikkawa, F. Kagawa, Y. Tokunaga, H. M. Rønnow, Y. Tokura, Y. Taguchi, *Nat. Mater.* **2016**, *15*, 1237.
- [21] L. Peng, Y. Zhang, W. Wang, M. He, L. Li, B. Ding, J. Li, Y. Sun, X.-G. Zhang, J. Cai, S. Wang, G. Wu, B. Shen, *Nano Lett.* **2017**, *17*, 7075.
- [22] M. He, L. Peng, Z. Zhu, G. Li, J. Cai, J. Li, H. Wei, L. Gu, S. Wang, T. Zhao, B. Shen, Y. Zhang, *Appl. Phys. Lett.* **2017**, *111*, 202403.
- [23] M. Uchida, Y. Onose, Y. Matsui, Y. Tokura, *Science* **2006**, *311*, 359.
- [24] R. Cheng, M. Li, A. Sapkota, A. Rai, A. Pokhrel, T. Mewes, C. Mewes, D. i Xiao, M. De Graef, V. Sokalski, *Phys. Rev. B* **2019**, *99*, 184412.
- [25] P. Jennings, P. Sutcliffe, *J. Phys. A: Math. Theor.* **2013**, *46*, 465401.
- [26] H.-J. Deiseroth, K. Aleksandrov, C. Reiner, L. Kienle, R. K. Kremer, *Eur. J. Inorg. Chem.* **2006**, *2006*, 1561.
- [27] A. F. May, S. Calder, C. Antoni, H. Cao, M. A. Mcguire, *Phys. Rev. B* **2016**, *93*, 014411.
- [28] Y. Deng, Y. Yu, Y. Song, J. Zhang, N. Z. Wang, Z. Sun, Y. Yi, Y. i Z. Wu, S. Wu, J. Zhu, J. Wang, X. H. Chen, Y. Zhang, *Nature* **2018**, *563*, 94.
- [29] A. F. May, D. Ovchinnikov, Q. Zheng, R. Hermann, S. Calder, B. Huang, Z. Fei, Y. Liu, X. Xu, M. A. Mcguire, *ACS Nano* **2019**, *13*, 4436.
- [30] A. F. May, C. A. Bridges, M. A. Mcguire, *Phys. Rev. Mater.* **2019**, *3*, 104401.
- [31] J. Stahl, E. Shlaen, D. Johrendt, *Z. Anorg. Allg. Chem.* **2018**, *644*, 1923.
- [32] N. Gao, S.-G. Je, M.-Y. Im, J. W. Choi, M. Yang, Q. Li, T. Y. Wang, S. Lee, H.-S. Han, K.-S. Lee, W. Chao, C. Hwang, J. Li, Z. Q. Qiu, *Nat. Commun.* **2019**, *10*, 5603.
- [33] T. Asaka, T. Kimura, T. Nagai, X. Z. Yu, K. Kimoto, Y. Tokura, Y. Matsui, *Phys. Rev. Lett.* **2005**, *95*, 227204.
- [34] N. Nagaosa, J. Sinova, S. Onoda, A. H. Macdonald, N. P. Ong, *Rev. Mod. Phys.* **2010**, *82*, 1539.
- [35] Y. Wang, C. Xian, J. Wang, B. Liu, L. Ling, L. Zhang, L. Cao, Z. Qu, Y. Xiong, *Phys. Rev. B* **2017**, *96*, 134428.
- [36] Y. Li, N. Kanazawa, X. Z. Yu, A. Tsukazaki, M. Kawasaki, M. Ichikawa, X. F. Jin, F. Kagawa, Y. Tokura, *Phys. Rev. Lett.* **2013**, *110*, 117202.